CHEMISTRY
A EUROPEAN JOURNAL

DOI: 10.1002/chem.201000616

Preparation of Core–Shell-Structured Nanoparticles (with a Noble-Metal or Metal Oxide Core and a Chromia Shell) and Their Application in Water Splitting by Means of Visible Light

Kazuhiko Maeda,[a] Naoyuki Sakamoto,[a] Takahiro Ikeda,[b] Hajime Ohtsuka,[b] Anke Xiong,[a] Daling Lu,[c] Masayuki Kanehara,[b] Toshiharu Teranishi,[b] and Kazunari Domen*[a]

Abstract: Core–shell-structured nanoparticles, consisting of a noble metal or metal oxide core and a chromia (Cr_2O_3) shell, were studied as promoters for photocatalytic water splitting under visible light. Core nanoparticles were loaded by impregnation, adsorption or photodeposition onto a solid solution of gallium nitride and zinc oxide (abbreviated GaN:ZnO), which is a particulate semiconductor photocatalyst with a band gap of approximately 2.7 eV, and a Cr_2O_3 shell was formed by photodeposition using a K_2CrO_4 precursor. Photodeposition of Cr_2O_3 on GaN:ZnO modified with a noble metal (Rh, Pd and Pt) or metal oxide (NiO_x, RuO_2 and Rh_2O_3) co-catalyst resulted in enhanced photocatalytic activity for overall water splitting under visible light ($\lambda > 400$ nm). This enhancement in activity was primarily due to the suppression of undesirable reverse reactions (H_2–O_2 recombination and/or O_2 photoreduction) and/or protection of the core component from chemical corrosion, depending on the core type. Among the core materials examined, Rh species exhibited relatively high performance for this application. The activity for visible-light water splitting on GaN:ZnO modified with an Rh/Cr_2O_3 core–shell configuration was dependent on both the dispersion of Rh nanoparticles and the valence state. In addition, the morphology of the Cr_2O_3 photodeposits was significantly affected by the valence state of Rh and the pH at which the photoreduction of K_2CrO_4 was conducted. When a sufficient amount of K_2CrO_4 was used as the precursor and the solution pH ranged from 3 to 7.5, Cr_2O_3 was successfully formed with a constant shell thickness (≈ 2 nm) on metallic Rh nanoparticles, which resulted in an effective promoter for overall water splitting.

Keywords: energy conversion · hydrogen · nanostructures · photochemistry · water chemistry

Introduction

Water splitting with visible light has been studied for the past four decades as a potential means of converting solar energy into chemical energy in the form of H_2.[1–9] Three proposed approaches to visible-light water splitting are illustrated in Scheme 1. The first (Scheme 1A) uses a single semiconductor photocatalyst, which should have a suitable thermodynamic potential for water splitting, a sufficiently narrow band gap to harvest visible photons and stability against photocorrosion.[5] The second (Scheme 1B) employs two different semiconductors and a reversible donor–acceptor pair (i.e., a shuttle redox mediator) that transfers electrons from one semiconductor to the other. This system was inspired by natural photosynthesis in green plants and is called the Z scheme.[3,8] In this system, a wide range of visible light is available, because the energy required to drive

[a] Dr. K. Maeda, N. Sakamoto, A. Xiong, Prof. Dr. K. Domen
Department of Chemical System Engineering
School of Engineering, The University of Tokyo
7-3-1 Hongo, Bunkyo-ku, Tokyo, 113-8656 (Japan)
Fax: (+81) 3-5841-8838
E-mail: domen@chemsys.t.u-tokyo.ac.jp

[b] T. Ikeda, H. Ohtsuka, Dr. M. Kanehara, Prof. Dr. T. Teranishi
Graduate School of Pure and Applied Sciences
University of Tsukuba
1-1-1 Tennoudai, Tsukuba, Ibaraki, 305-8571 (Japan)

[c] Dr. D. Lu
Center for Advanced Materials Analysis
Tokyo Institute of Technology
2-12-1 Ookayama, Meguro-ku, Tokyo 152-8550 (Japan)

Supporting information for this article is available on the WWW under http://dx.doi.org/10.1002/chem.201000616.

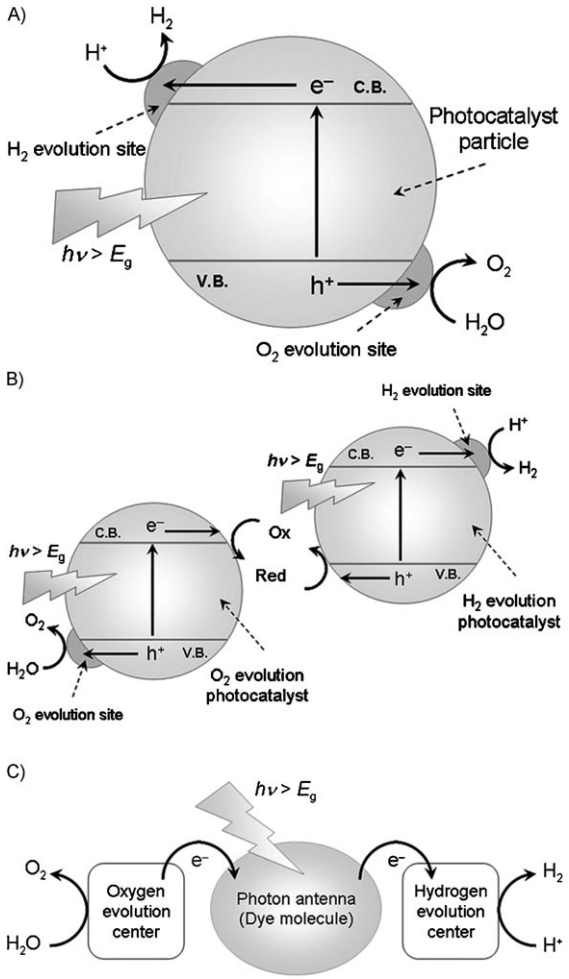

Scheme 1. Illustrations of visible-light water splitting (C.B. = conduction band; V.B. = valence band): A) One-step photoexcitation system with a single semiconductor material; B) two-step water splitting with two different semiconductor materials and a proper shuttle redox mediator; C) molecular building block approach with a light-harvesting antenna molecule and catalytic centres for H_2 and O_2 evolution.

each photocatalyst can be reduced. It is also possible to use a semiconductor with only a water reduction or oxidation potential for one side of the system. The last (Scheme 1C) is a molecular building block approach and is somewhat similar to the second scheme.[4,9] This system is composed of three essential components: a photon antenna and catalytic centres for hydrogen and oxygen evolution. It should be noted that all systems require catalysts to reduce the activation barrier for water reduction and/or oxidation. Catalysts, usually in the form of nanoparticles (so-called co-catalysts, especially in Scheme 1A and B), must be sufficiently active to promote the forward reaction, but remain inactive for reverse reactions (e.g., water formation from H_2 and O_2). For example, noble metals such as platinum and rhodium are excellent catalysts for H_2 formation. However, they also function as catalysts for water formation.

Recent progress in materials chemistry has advanced the development of such co-catalysts.[10–13] Our group attempted to develop a new water-reduction co-catalyst for Scheme 1A.[11–14] Among the promoters we have developed, core–shell-structured noble-metal/Cr_2O_3 nanoparticles dispersed on a photocatalyst were studied extensively, with a focus on their structural characteristics[11b] and functionality as active sites for H_2 evolution.[15] Based on a solid solution of GaN and ZnO as a semiconductor for the harvest of visible photons up to 500 nm,[16] the core–shell modification enables water splitting into H_2 and O_2 under visible light. In this system, the backward reaction over the noble metal (water formation from H_2 and O_2) is prevented by the Cr_2O_3 shell,[11a] because the amorphous Cr_2O_3 shell is permeable to protons and evolved H_2 molecules, but not to O_2.[15] This core–shell strategy is promising because it can be applied to other water-splitting systems, in which the suppression of H_2–O_2 recombination is a common requirement. Although this functionality is essential for a noble-metal-loaded photocatalyst to achieve overall water splitting,[11] it is not necessarily required for photocatalysts loaded with metal oxide because metal oxide co-catalysts generally exhibit negligible catalytic activity for water formation.[14b] In some cases, however, metal oxide co-catalysts sometimes undergo degradation due to a change in the co-catalyst state by exposure to the reactant solution, and catalyse O_2 photoreduction (another backward reaction of water splitting), which leads to a decrease in activity.[14b,17] When the loaded metal oxide nanoparticles are covered with Cr_2O_3, this deactivation and O_2 photoreduction should be suppressed by a reduced accessibility of the loaded metal oxides to the reactants. This idea stimulated our investigation of the activity of a photocatalyst loaded with metal oxide and modified with Cr_2O_3 photodeposits for overall water splitting.

In these core–shell co-catalysts, the physicochemical state of the core seems to be important, because the core loaded directly on a photocatalyst induces photogenerated electrons from the conduction band of the photocatalyst and hosts active sites for H_2 evolution. As described in our brief report, the water-splitting activity of GaN:ZnO modified with noble-metal/Cr_2O_3 core–shell nanoparticles was improved when highly dispersed noble-metal nanoparticles were loaded on GaN:ZnO without aggregation.[13] This result suggests that the activity of a core–shell system depends primarily upon the dispersion of the employed core. However, it is probable that other factors, such as the valence state of the core, can also affect the activity.

In the present study, we examined the core component of core–shell-structured nanoparticle co-catalysts for visible-light water splitting. First, we report the photocatalytic activities of GaN:ZnO modified with nanoparticulate noble-metal or metal oxide cores and Cr_2O_3 shells. Second, we examine the effects of the preparation conditions of the core–shell components on activity. Finally, factors affecting the water-splitting activity are discussed to establish guidelines for the preparation of highly active photocatalysts.

Results and Discussion

Characterisation of nanoparticulate metal oxides loaded on GaN:ZnO treated with K_2CrO_4 under visible light: Figure 1 shows high-resolution (HR) TEM images of NiO_x-, Rh_2O_3- and RuO_2-loaded GaN:ZnO before and after photoreduction treatment with K_2CrO_4. The introduced NiO_x nanoparticles were 5–8 nm in size and were crystalline, as indicated by the lattice fringes. Upon photodeposition, the size of the nanoparticles dispersed on GaN:ZnO became larger and more irregular in shape, and it was difficult to identify the interface between the NiO_x and the photodeposited Cr species. Nevertheless, energy-dispersive spectroscopy (EDS) analysis revealed that the nanoparticles after photodeposition contained both Ni and Cr, which indicated that photoreduction of K_2CrO_4 and subsequent photodeposition of Cr species both occurred on the NiO_x nanoparticles. Note that almost no reduction of K_2CrO_4 on the GaN:ZnO surface occurred, due primarily to the lack of adsorption sites on GaN:ZnO.[11b] An identical tendency was observed for Rh_2O_3-loaded GaN:ZnO. In contrast, core–shell-like nanostructures were clearly observed in RuO_2-loaded GaN:ZnO after the treatment. RuO_2 on GaN:ZnO formed crystalline nanoparticles ranging from 2 to 20 nm in size, as indicated by the clear lattice fringes, whereas the shell exhibited an amorphous structure and produced no lattice fringes. It should also be noted that some of the loaded RuO_2 nanoparticles remained uncoated, even though a significant amount of K_2CrO_4 coexisted in the reactant solution. This indicates that some of the RuO_2 nanoparticles loaded on GaN:ZnO did not function as reduction sites for CrO_4^{2-} anions, while others promoted the reduction of both CrO_4^{2-} anions and protons. One possible explanation for this phenomenon is that the uncoated RuO_2 functioned as water oxidation sites throughout the photodeposition treatment process. The idea that RuO_2 on GaN:ZnO facilitates both water reduction and water oxidation during photocatalytic water splitting is supported by our previous studies.[14b,e]

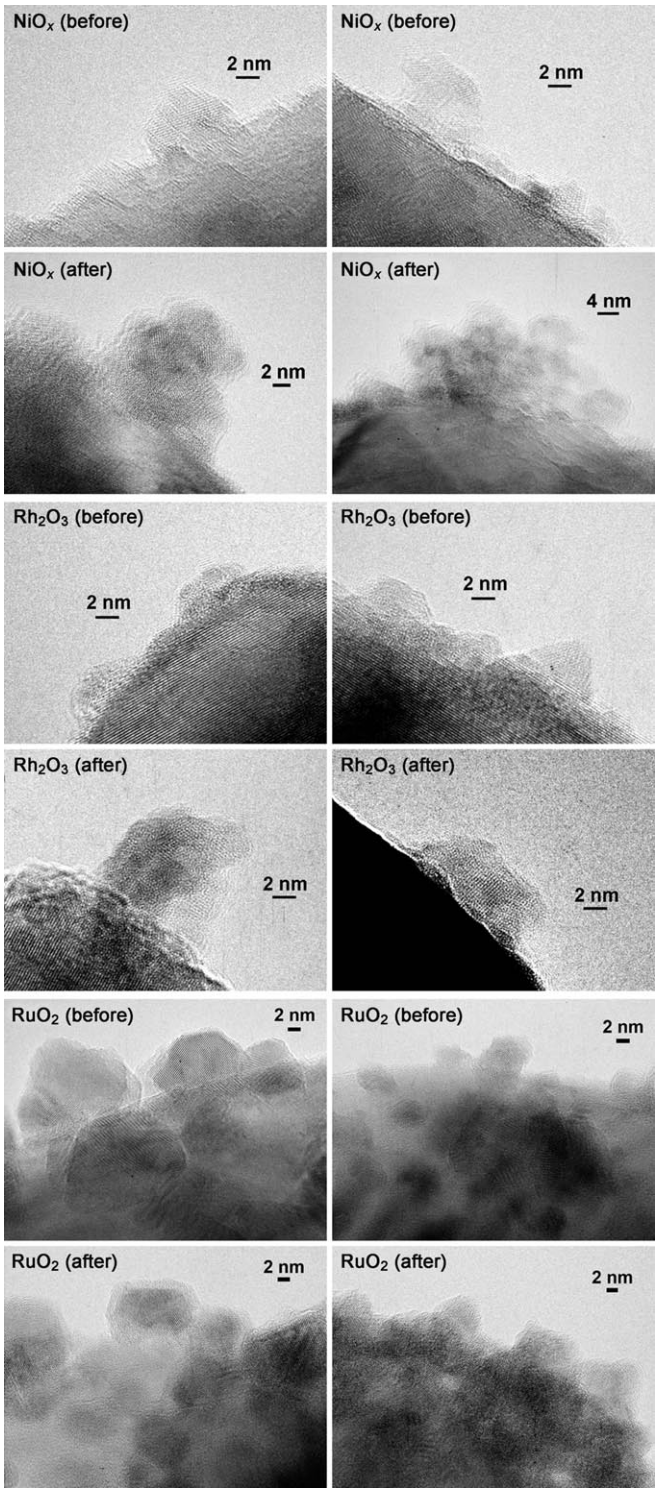

Figure 1. TEM images of NiO_x-, Rh_2O_3- and RuO_2-loaded GaN:ZnO before and after treatment with K_2CrO_4 at pH 7.5 under visible light.

The valence state of the deposited Cr species in the catalysts was investigated by X-ray absorption fine structure (XAFS) spectroscopy. Figure 2A shows the Cr K-edge X-ray absorption near-edge structure (XANES) spectra for GaN:ZnO modified with metal oxides after photodeposition of Cr species. The data for Cr_2O_3 and K_2CrO_4 are shown for comparison. The Cr near-edge spectrum for K_2CrO_4 exhibited a sharp pre-edge feature at approximately 5992 eV resulting from dipole-forbidden 1s to 3d transitions, which was assigned to hexavalent Cr.[18] This pre-edge feature was negligible in the spectrum of Cr_2O_3. The Cr K-edge spectra of all prepared samples differed from those of K_2CrO_4. The spectral region around the absorption edge and approximately 6020 eV in the samples resembled that of the Cr_2O_3 reference, although a small pre-edge peak assigned to hexavalent Cr was observed for the NiO_x sample. Figure 2B shows the Cr K-edge extended X-ray absorption fine structure (EXAFS) spectra of the same samples, along with data for Cr_2O_3 and K_2CrO_4. The EXAFS spectra of the samples were identical and were similar to that of Cr_2O_3, judging from the appearance of the Cr–O shell at approximately 1.7 Å. The relatively weak peak at approximately 2.5 Å, assignable to the Cr-(O)-Cr shell, suggests a small size, which was supported by TEM observations. These results indicate

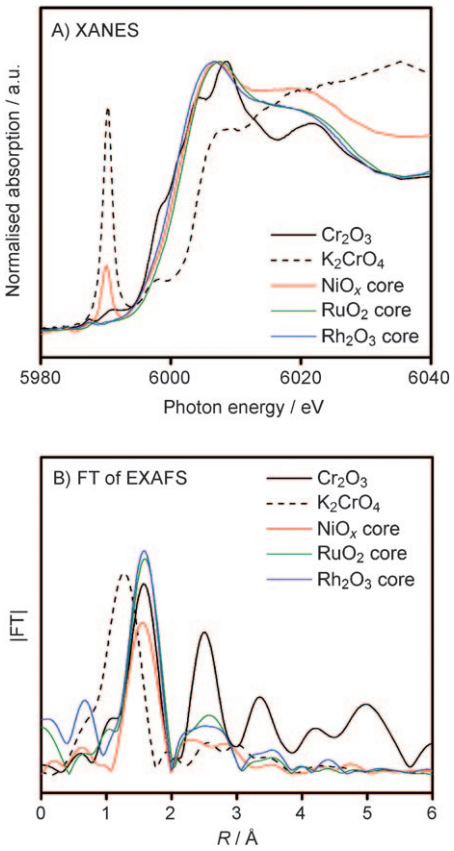

Figure 2. A) Cr K-edge XANES and B) Fourier transforms of k^3-weighted EXAFS spectra for Rh-loaded GaN:ZnO treated with K_2CrO_4 at pH 7.5 under visible light.

that the Cr species in the catalysts were deposited entirely in the trivalent oxide form (Cr_2O_3), regardless of the transition-metal oxide type, although the NiO_x sample contained a small fraction of hexavalent Cr species.

Photocatalytic activity of metal oxide (core) modified GaN:ZnO with Cr_2O_3 shells: Table 1 lists the photocatalytic activities for visible-light-driven overall water splitting on NiO_x-, RuO_2- and Rh_2O_3-loaded GaN:ZnO, before and after photodeposition of Cr_2O_3. These metal oxides have previously been reported as co-catalysts for overall water splitting.[7,19,20] As reported previously, NiO_x- and RuO_2-loaded GaN:ZnO produced H_2 and O_2 in stoichiometric amounts, whereas the Rh_2O_3-loaded analogue exhibited little activity.[14,21] However, upon photodeposition of Cr_2O_3, the activities of these catalysts were enhanced in all cases and the gas evolution behaviours varied more or less. Figure 3 shows time courses of overall water splitting under visible-light irradiation on NiO_x-loaded samples, before and after photodeposition of Cr_2O_3. The rates of H_2 and O_2 evolution decreased gradually with reaction time and became constant (7.4 μmol h^{-1} for H_2 evolution and 3.6 μmol h^{-1} for O_2 evolution) in the second run. In contrast, NiO_x-loaded samples modified with Cr_2O_3 photodeposits produced H_2 and O_2 proportionally and stoichiometrically from the beginning of the reaction, although an induction period was observed in the first run, presumably due to the reduction of remnant Cr^{VI} to Cr^{III}, as supported by the XANES analysis (Figure 2). The steady rates of gas evolution on the Cr_2O_3-photodeposited catalyst were two times higher than those observed without Cr_2O_3 photodeposits.

It is likely that the deactivation of the NiO_x-loaded sample was primarily due to a change in the state of NiO_x on the catalyst surface, which has been observed in some NiO-loaded photocatalysts for overall water splitting. Kato and Kudo reported that immersion of NiO-loaded $NaTaO_3$ in pure water causes NiO nanoparticles to peel off or elute as $Ni(OH)_2$, even without irradiation, resulting in gradual

Table 1. Photocatalytic activity for visible-light-driven overall water splitting on GaN:ZnO modified with various co-catalysts.[a]

Entry	Co-catalyst	Cr_2O_3 photodeposition	Activity[b] [μmol h^{-1}] H_2	O_2
1	NiO_x	no	7.4	3.6
2		yes	15	7.4
3	RuO_2	no	36	18
4		yes	47	24
5	Rh_2O_3	no	1.4	trace
6		yes	70	36
7	Rh[c]	no	<1	<1
8		yes	179	88
9	Pd[c]	no	<1	<1
10		yes	15	5.2
11	Pt[c]	no	<1	<1
12		yes	32	16
13	Rh[c]	[d]	4.1	1.5

[a] Reaction conditions: catalyst, 0.15 g; distilled water, 370–400 mL; light source, high-pressure mercury lamp (450 W) through an aqueous $NaNO_2$ solution filter to cut ultraviolet light; reaction vessel, Pyrex inner-irradiation type. [b] Steady rate of gas evolution. [c] Metal (1.0 wt % addition) was loaded by photodeposition. [d] A mixture of Rh-loaded GaN:ZnO with Cr_2O_3 treatment (0.15 g) and without this treatment (0.15 g) was used.

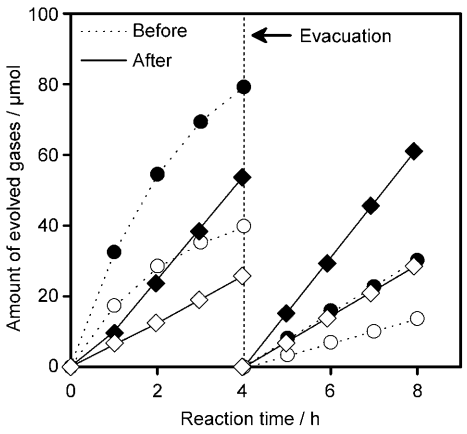

Figure 3. Time courses of visible-light-driven overall water splitting on NiO_x-modified GaN:ZnO with (circles) or without K_2CrO_4 treatment (diamonds). Reaction conditions: catalyst, 0.15 g; distilled water, 370 mL; light source, high-pressure mercury lamp (450 W) through an aqueous $NaNO_2$ solution filter to cut ultraviolet light; reaction vessel, Pyrex inner-irradiation type. Solid and open symbols indicate H_2 and O_2, respectively.

deactivation of the catalyst.[17] In contrast, NiO_x-loaded GaN:ZnO photodeposited with Cr_2O_3 produced H_2 and O_2 proportionally and stoichiometrically without any noticeable deactivation as the reaction progressed, and the steady rates of H_2 and O_2 evolution were higher than those without Cr_2O_3 photodeposits. According to HR-TEM observations and EDS measurements, it appeared that Cr_2O_3 photodeposits coated NiO_x nanoparticles dispersed on GaN:ZnO. This would help protect from deactivation of the NiO_x nanoparticles, thus enhancing their activity. When we examined the Ni K-edge XANES spectra for samples with and without Cr_2O_3 photodeposition after the water-splitting reaction, there was almost no change between the two samples (Figure S1 in the Supporting Information). Such a chemical change during photoreaction would probably be too subtle to detect.

The Cr_2O_3 photodeposition method was also found to effectively improve the activity for overall water splitting of RuO_2- and Rh_2O_3-loaded GaN:ZnO, as listed in Table 1, but both RuO_2 and Rh_2O_3 are stable in neutral aqueous solution.[22] Therefore, it is likely that the reason for this activity improvement was not the suppression of a chemical change, but some other factor. We have previously reported that the photoreduction of O_2 on RuO_2-loaded GaN:ZnO occurs during water splitting under visible light.[14b] As mentioned earlier, a Cr_2O_3 layer on a noble metal forms a selective proton- and H_2-permeable membrane that prevents O_2 penetration.[15] A similar phenomenon is expected in the Cr_2O_3/RuO_2/GaN:ZnO system; that is, the Cr_2O_3 layer on RuO_2 hinders the access of O_2 molecules to the RuO_2 surface without blocking protons or H_2 molecules, thereby improving the water-splitting activity. In fact, the rate of H_2 evolution in overall water splitting over Cr_2O_3/RuO_2/GaN:ZnO remained almost unchanged, even in the presence of O_2 gas (30 kPa). It was also revealed that the H_2 evolution activity of Cr_2O_3/RuO_2/GaN:ZnO from an aqueous methanol solution (O_2-free condition) is slightly lower (33 $\mu mol\,h^{-1}$) than that of RuO_2/GaN:ZnO (41 $\mu mol\,h^{-1}$), in contrast to the case of water splitting (Table 1). Therefore, it can be concluded that the Cr_2O_3 shell modification has a positive effect on water reduction by inhibiting O_2 photoreduction. Unfortunately, it was difficult to examine the photoreduction of O_2 on Rh_2O_3-loaded GaN:ZnO in a similar manner to RuO_2,[14b] because of its negligible activity for water splitting (Table 1). Nevertheless, Rh_2O_3-loaded GaN:ZnO is active for H_2 evolution from aqueous methanol under visible light (see Supporting Information Figure S2), which indicates that Rh_2O_3 on GaN:ZnO functions as an H_2 evolution site under O_2-free conditions. The enhancement of water-splitting activity observed in the Rh_2O_3 system would thus occur by a similar mechanism to that of the RuO_2 system.

Table 1 also lists visible-light-driven water-splitting activities of Rh-photodeposited GaN:ZnO before and after photodeposition of Cr_2O_3. As reported previously, Rh-photodeposited GaN:ZnO exhibits little activity (entry 7), whereas treatment of this material with Cr_2O_3 results in an appreciable increase in activity (entry 8).[11] The identical trend was observed in Pd- and Pt-photodeposited GaN:ZnO (entries 9–12). As mentioned in the Introduction, noble metals act as efficient catalysts to produce H_2O from H_2 and O_2. Although the photoreduction of O_2 also proceeds on the surface of noble metals,[15] this marked improvement in activity is most likely due to the suppression of water formation. This idea is further supported by the observation that the addition of Rh-loaded GaN:ZnO powder into the active photocatalyst (Rh-loaded GaN:ZnO with Cr_2O_3 photodeposition) led to a significant drop in activity (entry 13). This indicates that gaseous H_2 and O_2 molecules produced on the active photocatalyst efficiently undergo recombination on Rh-loaded GaN:ZnO before they escape from the reactant suspension.

The Cr_2O_3-photodeposition method was thus shown to be applicable not only to noble metals,[11] but also to metal oxides for improving the photocatalytic activity for overall water splitting, although an ideal core–shell-like structure, as observed in noble-metal/Cr_2O_3 systems, could not be formed. It is concluded that the mechanism by which the Cr_2O_3 deposits improve the water-splitting activity depends upon the core type. A notable feature of Table 1 is that Rh species can function as a good core component, but the metal oxide (Rh_2O_3) had a lower performance ($\approx$70 $\mu mol\,h^{-1}$ for H_2 evolution, entry 6) than that of metallic Rh ($\approx$180 $\mu mol\,h^{-1}$ for H_2 evolution, entry 8). This implies that the valence state of Rh also affects the water-splitting activity and that metallic Rh is a superior core material. Therefore, the effects of the preparation method of metallic Rh nanoparticles are examined in the following section.

Water-splitting activity and structural characteristics of GaN:ZnO modified with Rh/Cr_2O_3 core–shell nanoparticles: Table 2 lists the photocatalytic activity for visible-light water splitting on GaN:ZnO modified with Rh nanoparticles and subsequently treated with K_2CrO_4 and visible light. The Rh

Table 2. Photocatalytic activity of Cr_2O_3/Rh/GaN:ZnO for overall water splitting under visible-light irradiation ($\lambda > 400$ nm).[a]

Entry	Loading method for Rh core	Amount of Rh added [wt%]	Activity[b] [$\mu mol\,h^{-1}$] H_2	O_2
1		0	0	0
2	photodeposition	0.5	131	69
3		1.0	179	88
4		1.5	150	75
5	impregnation	0.1	17	7.9
6		0.25	149	72
7		0.5	115	56
8		1.0	91	45
9	adsorption	0.5	220	109
10		1.0	336	168
11		1.5	384	191
12		2.0	378	190
13		2.5	426	213
14		3.0	390	195

[a] Reaction conditions: catalyst, 0.15 g; distilled water, 370–400 mL; light source, high-pressure mercury lamp (450 W) through an aqueous $NaNO_2$ solution filter to cut ultraviolet light; reaction vessel, Pyrex inner-irradiation type. [b] Average rates after 5 h of reaction.

nanoparticles were introduced onto the GaN:ZnO by photodeposition, impregnation or adsorption, in varying amounts. Without adding Rh, no gas evolution was detected (entry 1). However, modification of GaN:ZnO with Rh nanoparticles resulted in observable H_2 and O_2 evolution in a nearly stoichiometric ratio ($H_2/O_2 \approx 2$), which indicates that overall water splitting occurred in all cases. In the samples prepared by photodeposition or impregnation, a volcano-type relationship was observed between the loading amount of Rh and activity; specifically, the activity increased with increasing Rh addition up to a certain level, beyond which it began to decline. On the other hand, the rates of H_2 and O_2 evolution on the samples prepared by adsorption reached saturation at approximately 400 $\mu mol\,h^{-1}$ H_2 and 200 $\mu mol\,h^{-1}$ O_2. The highest activity was obtained with the sample prepared by adsorption with an Rh addition of 1.5–3.0 wt%. Thus, adsorption was found to be superior to photodeposition and impregnation for the preparation of water-splitting photocatalysts.

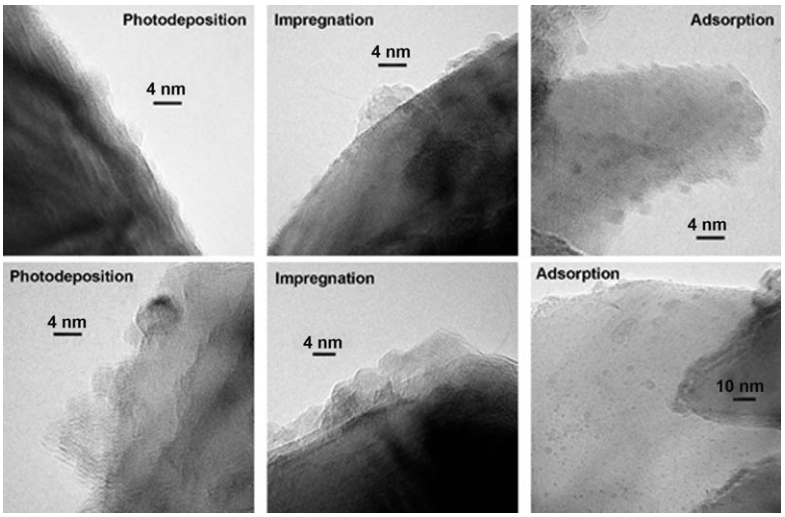

Figure 4. TEM images of Rh-loaded GaN:ZnO prepared by means of different routes.

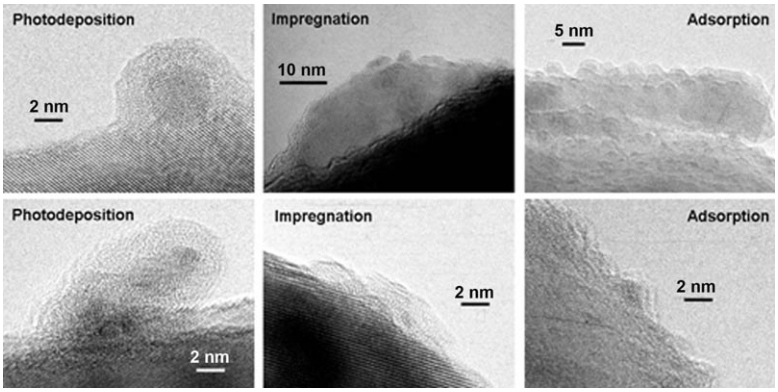

Figure 5. TEM images of Rh-loaded GaN:ZnO treated with K_2CrO_4 at pH 7.5 under visible light.

The differences in activity among the samples prepared by means of the above three routes is expected to be attributed to the different structural characteristics of the samples. Figure 4 shows HR-TEM images of samples prepared under the optimal conditions for each method. As reported previously, the primary particle size of photodeposited Rh nanoparticles was 2–3 nm, but some of them aggregated to form larger secondary particles.[11a] Samples prepared by impregnation had a similar tendency. In addition to approximately 2 nm nanoparticles, agglomerates larger than 10 nm in size were observed. In contrast to these two samples, the sample prepared by adsorption exhibited excellent dispersion of primary Rh nanoparticles and very little aggregation was identified. The average Rh particle size on this sample was calculated to be (1.9 ± 0.6) nm (based on 200 different particles).

TEM images of the same set of samples after treatment with K_2CrO_4 and visible light are shown in Figure 5. As reported previously, a Cr_2O_3 shell with a constant thickness of approximately 2 nm covered photodeposited Rh nanoparticles on GaN:ZnO after this treatment, producing core–shell-structured Rh/Cr_2O_3 nanoparticles. The Cr_2O_3 shell thickness was totally independent of the dispersion of Rh, although a given concentration of K_2CrO_4 was required to afford a constant shell thickness of approximately 2 nm.[11b] Interestingly, such a core–shell-like structure was rarely observed in impregnated samples, in which featureless particles were instead dominant. Nevertheless, energy dispersive X-ray analysis detected the coexistence of Rh and Cr in these featureless particles, which indicated that the photodeposition of Cr species did occur on Rh nanoparticles introduced by impregnation. In the adsorbed samples, most nanoparticles had a core–shell structure, but some irregular-shaped shell structures were also observed. Therefore, the dispersion of Rh and the morphology of Cr photodeposits varied with respect to the preparation method of the Rh nanoparticles.

The valence states of Rh and Cr in the composite materials were investigated by XAFS measurements. Figure 6A shows the Rh K-edge XANES spectra for each optimised sample. Data for an Rh foil and Rh_2O_3 are shown for reference. The Rh K-edge XANES spectra for the prepared sam-

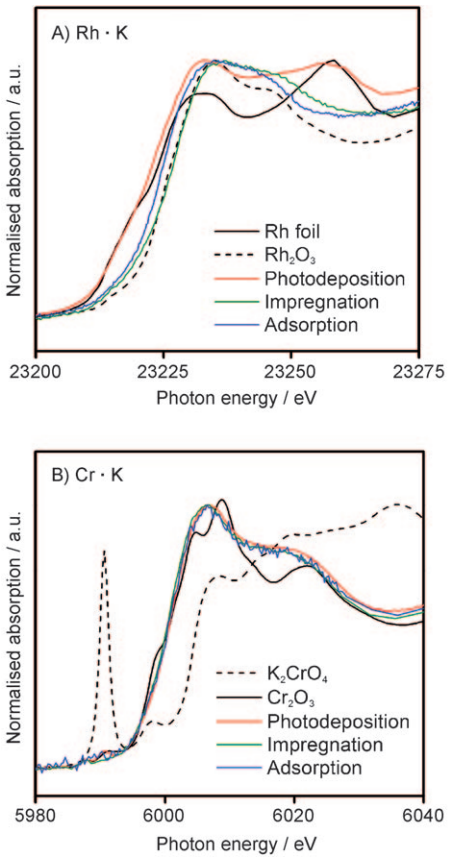

Figure 6. A) Rh K- and B) Cr K-edge XANES spectra for Rh-loaded GaN:ZnO treated with K_2CrO_4 at pH 7.5 under visible light.

ples were dissimilar to each other, indicating different valence states of Rh. The position of the absorption edge of the photodeposited sample was very close to that of the Rh foil and the spectral shape around the absorption maximum and at 23260 eV were similar. This indicates that the valence state of Rh in the photodeposited sample was nearly metallic. This is further supported by Fourier transforms of the k^3-weighted EXAFS spectrum from the same sample.[11b] The absorption-edge position of the impregnated sample was at a slightly lower photon energy than the Rh_2O_3 reference, while the adsorbed sample had an absorption edge at a position between those of the Rh foil and the Rh_2O_3. The Rh K-edge XANES spectrum of the impregnated sample was not completely consistent with that of the Rh_2O_3 reference, which indicates that Rh in the impregnated sample had a valence state close to that of Rh_2O_3, but slightly reduced. Overall, the XANES analysis indicated that the valence state of Rh in the composite samples prepared by different methods becomes closer to metallic in the order of impregnation→adsorption→photodeposition. Furthermore, there was no significant difference in the Rh K-edge XANES spectra before and after K_2CrO_4 treatment (Figure S3 in the Supporting Information), which indicates that the valence state of Rh was maintained throughout the treatment process, regardless of the preparation method.

In contrast to the Rh K-edge spectra, the Cr K-edge XANES spectra were all identical, regardless of the preparation method, as shown in Figure 6B. Although the spectral shape of the prepared samples was not completely consistent with either K_2CrO_4 or Cr_2O_3, the absorption edges were all at the same position as that of Cr_2O_3. This is consistent with the behaviour of metal oxide core systems (Figure 2). For the photodeposited sample, it was determined by X-ray photoelectron spectroscopy (XPS) that the positions of the Cr 2p peaks were consistent with those of the Cr_2O_3 reference.[11b] Therefore, the valence state of Cr in the samples was trivalent and was independent of the nanoparticulate core type and morphology.

The thickness of the Cr_2O_3 shell was also dependent on the pH of the solution in which the photoreduction of K_2CrO_4 was conducted. As a result, the water-splitting activity of samples prepared at different pH were different (Figure S4 in the Supporting Information). When the deposition pH ranged from 3.0 to 7.5, there was almost no change in activity and stoichiometric H_2 and O_2 were produced under visible light. As the pH decreased from 3.0 to 2.0, however, the rates of H_2 and O_2 evolution both decreased significantly. TEM observations showed that, in the Rh-photodeposited GaN:ZnO treated with K_2CrO_4 and visible light at pH 2.0, almost no core–shell-like structure could be identified (Figure S5 in the Supporting Information), in contrast to the sample treated at pH 7.5 (Figure 5). Nevertheless, the yellow colour of the initial solution, which was due to K_2CrO_4, disappeared completely and turned a faint dark blue, the typical colour of Cr^{III} sulfate. This indicates that the photoreduction of Cr^{VI} ions occurred at this pH condition, but at this low pH the Cr^{III} ions could not precipitate as Cr^{III} hydroxide or oxide. Therefore, a relatively neutral pH is a better choice when coating nanoparticulate cores with Cr_2O_3 shells.

Factors affecting the activity: Our previous brief report suggested that the dispersion of Rh nanoparticles is an important factor affecting the activity for overall water splitting under visible light, because it determines the density of available active surface for H_2 evolution.[13] The results obtained in the present study further support this idea. In fact, the adsorbed sample with a relatively high dispersion of Rh nanoparticle cores exhibited a higher activity than samples prepared by photodeposition or impregnation, in which the Rh nanoparticles were poorly dispersed (Table 2 and Figure 4).

It is notable that there is a trade-off between the amount of Rh added and the activity of photodeposited or impregnated samples, but the activity of samples prepared by adsorption saturates at a certain level of Rh addition. In impregnated samples, for example, it was evident from the SEM images that the density of the introduced Rh nanoparticles on the GaN:ZnO surface increased with increasing addition of Rh, as shown in Figure 7. The colour of the prepared sample was yellowish green, which turned denser with increasing Rh addition, indicating an increased density of

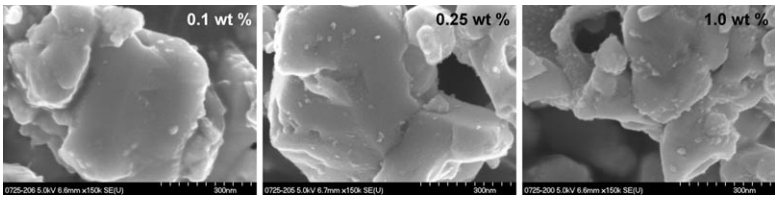

Figure 7. SEM images of Rh-loaded GaN:ZnO prepared by impregnation, followed by H_2 reduction at 523 K for 2 h.

Rh on the GaN:ZnO. The abrupt increase in activity with Rh addition from 0 to 0.25 wt% was therefore attributed to an increase in the density of active sites for H_2 evolution. On the other hand, the decrease in activity at higher Rh loadings is probably related to excess coverage of the Rh nanoparticles deposited on GaN:ZnO, as supported by SEM observations. Such excess loading can cause an inner-filter effect, contributing to a decrease in activity.[23–26] Another possibility is that electron–hole recombination on the surface of the Rh catalyst, which was indicated by our recent spectroscopic study,[27] increases at higher loading, contributing to a decrease in H_2 evolution activity.

In the samples prepared by adsorption, the saturation of activity occurred because the amount of introduced Rh nanoparticles reached saturation at 0.3–0.4 wt% for 1.5–3.0 wt% addition, according to inductively coupled plasma atomic emission spectroscopy (ICP-AES) analysis. Therefore, during the loading process, Rh nanoparticles stabilised by organic ligands are introduced onto GaN:ZnO by means of adsorption–desorption. Specifically, hydrogen-bonding and/or acid–base interaction between sulfonic acid groups on the Rh nanoparticles and surface hydroxyl and amino groups on the GaN:ZnO both play important roles. Zhang et al. suggested the presence of N−H bonds on the surface of GaN epilayers grown by molecular beam epitaxy on the basis of a splitting of the N 1s photoelectron signal in their XPS analysis.[28] Baraton and Gonsalves conducted infrared spectroscopy analysis of GaN powder and found that GaN has NH, NH_2 and OH groups on its surface.[29] The N 1s XPS peak of the GaN:ZnO used in the present study can also be resolved into two peaks (Figure S6 in the Supporting Information). The major peak is assignable to metal–nitrogen bonding in the lattice, whereas the minor one, which appeared at higher binding energy, derives from surface N−H bonding, according to a previous XPS study of GaN.[28] Therefore, it is reasonable to conclude that sulfonic acid groups on the Rh nanoparticles interact with hydroxyl and/or amino groups on the GaN:ZnO surface by means of hydrogen bonding and/or acid–base interaction. This idea is further supported by the observation that sulfonate-terminated Rh nanoparticles do not adsorb onto GaN:ZnO. As a result, the amount of Rh thus introduced onto the surface of GaN:ZnO is limited to a certain level.

Rh species in the sample extract photogenerated electrons from the conduction band of GaN:ZnO and host active sites for H_2 evolution.[14] Therefore, not only the dispersion of Rh but also the valence state should be important. XANES analysis determined that the valence state of Rh in the samples tended towards metallic in the order of impregnation→adsorption→photodeposition, as indicated by the Rh K-edge XANES spectra (Figure 6A). A previous study indicated that metallic Rh is superior to the oxidised state, both as an electron collector from GaN:ZnO and as an H_2 evolution site.[12b] As listed in Tables 1 and 2, the activity of the Rh_2O_3 (core) sample[30] (entry 6, Table 1) was 20% lower than that of the sample prepared in a similar manner but with H_2-reduction treatment (entry 8, Table 2), thereby confirming that metallic Rh is a better co-catalyst for H_2 evolution than the oxidised state. We also attempted to promote the reduction of Rh species introduced by impregnation by increasing the temperature in the treatment procedure. Unfortunately, however, increasing the reduction temperature beyond 523 K resulted in a decrease in activity (data not shown here). Presumably, the surface of the GaN:ZnO was damaged by the treatment, because Zn^{2+} species in the solid surface are susceptible to reduction.[16b,31] For this reason, the impregnation method was not effective for the loading of Rh nanoparticles onto GaN:ZnO.

On the basis of these results, the excellent activity of the adsorbed samples can be attributed to a high dispersion of Rh, even though some of the Rh nanoparticles are likely to be oxidised. It is also preferable for the Rh nanoparticle core to be in a metallic state, but this appears to be a secondary factor affecting the activity. By utilizing interactions between the organic groups on the noble-metal nanoparticles and surface functional groups on a photocatalyst, the loading of highly dispersed noble-metal nanoparticles was demonstrated to be possible. Our preliminary experiments have demonstrated that various combinations of a noble-metal nanoparticle and a support (e.g., Au-loaded GaN:ZnO, Rh-loaded TiO_2 and so on) can be prepared with uniform dispersion by modifying the protecting ligands of the noble-metal nanoparticles. These results will be published elsewhere as part of our future work.

Conclusion

Photodeposition of Cr_2O_3 onto nanoparticulate NiO_x, RuO_2 and Rh_2O_3 dispersed on GaN:ZnO was shown to be an effective approach to improve the activity for overall water splitting under visible light. Suppressing undesirable chemical changes of a co-catalyst and/or O_2 photoreduction are likely to contribute to this enhanced photocatalytic activity. Therefore, Cr_2O_3 photodeposition can improve H_2 evolution, not only on noble metals but also on metal oxides.

The introduction of an Rh species core onto GaN:ZnO yielded a relatively high activity for visible-light water splitting when coated with Cr_2O_3. High dispersion and non-ag-

gregation of the Rh nanoparticles are the most important factors in the enhanced activity of Cr_2O_3/Rh/GaN:ZnO. Furthermore, the morphology of the Cr_2O_3 photodeposits on the Rh nanoparticles was dependent on the valence state of the Rh and the pH of the solution in which the shell was formed, but independent of the dispersion of Rh. The shell thickness of the Cr_2O_3 photodeposited on Rh became less uniform as the valence state of the Rh changed from metallic to a trivalent oxide.

Experimental Section

Materials and reagents: GaN:ZnO solid solution semiconductor photocatalyst supports were prepared according to the method described previously.[16] Briefly, a mixture of Ga_2O_3 and ZnO powders (1.08 g Ga_2O_3 and 0.94 g ZnO) was heated to 1123 K under an NH_3 flow (250 mL min^{-1}). After 15 h of nitridation, the sample was cooled to room temperature, while maintaining the NH_3 flow throughout. Elemental analysis by ICP revealed that the material contained Ga (43.9 at%), Zn (6.4 at%), N (41.9 at%) and O (7.9 at%).[16a] The production of GaN:ZnO was confirmed by powder X-ray diffraction (XRD) and energy-dispersive X-ray (EDX) analysis. The band-gap energy of the as-obtained GaN:ZnO was 2.68 eV, as estimated from the onset of the diffuse reflectance spectrum. The particle size was typically 200–500 nm, as indicated by scanning electron microscopy.[16b] The specific surface area determined by nitrogen adsorption at 77 K was approximately 7.4 m^2 g^{-1}.[16b]

$Ni(NO_3)_2{\cdot}6H_2O$ (Kanto Chemicals, 98%), $[Ru_3(CO)_{12}]$ (Aldrich Chemical Co., 99%), $Na_3RhCl_6{\cdot}2H_2O$ (Kanto Chemicals, 97% as Rh), $Na_3RhCl_6{\cdot}12H_2O$ (Mitsuwa Chemicals, 99.9%), $Rh(NO_3)_3$ (Kanto Chemicals, 99.9%), $RhCl_3$ (Aldrich Chemical Co., 99.98%), sodium 3-mercapto-1-propanesulfonate (Tokyo Chemical Industry Co., 80%), $NaBH_4$ (Kanto Chemicals, 92%) and K_2CrO_4 (Kanto Chemicals, 99%) were used as precursors to prepare the core–shell-structured nanoparticles without further purification. In measurements of XAFS and XPS spectra, Rh_2O_3 (Kanto Chemicals, 99.9%), Cr_2O_3 (Kanto Chemicals, 98.5%) and K_2CrO_4 were used as references.

Modification of GaN:ZnO with nanoparticulate metal oxides: Nanoparticulate transition-metal oxide (NiO_x, RuO_2 and Rh_2O_3) cores were loaded onto as-prepared GaN:ZnO by impregnation.[14] For NiO_x and Rh_2O_3, 0.3–0.4 g of GaN:ZnO powder and 3–4 mL of distilled water containing an appropriate amount of $Ni(NO_3)_2{\cdot}6H_2O$ or $Rh(NO_3)_3$ were placed in an evaporating dish on a water bath. The suspension was evaporated under constant stirring by using a glass rod until complete dryness was reached. For NiO_x loading, the impregnated catalyst was reduced by exposure to H_2 (20 kPa) at 573 K for 2 h and then oxidised by exposure to O_2 (10 kPa) at 473 K for 1 h in a closed gas-circulation system.[14d,19] For Rh_2O_3, the impregnated powder was heated in air at 623 K for 1 h. NiO_x and Rh_2O_3 were loaded at rates of 1 wt% (metallic content). In the case of RuO_2, the GaN:ZnO powder was immersed in a solution containing dissolved $[Ru_3(CO)_{12}]$ in tetrahydrofuran (THF), followed by stirring at 333 K for 5 h. The solution was then dried under reduced pressure by heating in air at 373 K for 1 h to remove the THF. The resulting powder was finally heated in air at 623 K for 1 h to convert the Ru species to RuO_2 nanoclusters.[21] The RuO_2 loading achieved in this manner was 5 wt%.

Modification of GaN:ZnO with Rh nanoparticles: Modification of GaN:ZnO powder with nanoparticulate Rh to form the core was carried out by following three different methods—photodeposition, impregnation and adsorption—to investigate the effects of preparation conditions on photocatalytic activity. The preparation procedures are described below.

Photodeposition was conducted in a glass closed gas-circulation system. The powder was immersed in distilled water (370–400 mL) containing a given amount of Na_3RhCl_6. The suspension was evacuated to remove dissolved air completely and then irradiated with visible light for 4 h. After being filtered and washed with pure water, the resulting powder was dried in an oven at 343 K for 24 h.

In the impregnation method, GaN:ZnO powder (0.3–0.4 g) was immersed in an aqueous solution (3–4 mL) containing different amounts of $[Rh(NO_3)_3]$ and placed in a water bath. After evaporating the solution to dryness, the resulting powder was collected and heated with H_2 gas (20 kPa) at 473–623 K for 2 h in a glass closed gas-circulation system.

The adsorption method involved the preparation of nanoparticles by liquid-phase reduction of $RhCl_3$ in the presence of sodium 3-mercapto-1-propanesulfonate to obtain Rh nanoparticles stabilised by organic ligands. An aqueous solution containing equal molar amounts (15–90 μmol, corresponding to 0.5–3.0 wt% with respect to GaN:ZnO powder) of $RhCl_3$ and sodium 3-mercapto-1-propanesulfonate was prepared in a conical flask and reduced by $NaBH_4$ under air. The amount of $NaBH_4$ added to the solution was 10 times the amount of $RhCl_3$ employed. The as-prepared Rh nanoparticles were (1.7 ± 0.3) nm in size, as reported previously.[13] After purification, H-type Amberlyst was added to the solution to convert the terminal sulfonate groups to sulfonic acid groups. After removal of the Amberlyst by filtration, the nanoparticles were loaded onto the GaN:ZnO catalyst by adding the powder (0.300 g) to the solution. After letting the solution stand for 30 min, the organic ligands were eliminated by calcination under vacuum at 673 K for 30 min. Elemental analysis by X-ray fluorescence spectroscopy confirmed that sulfur species derived from organic ligands were completely eliminated by the calcination.

Photoreduction of Cr^{VI} to form Cr_2O_3 shells on nanoparticulate cores: The formation of Cr_2O_3 shells on nanoparticulate cores was carried out by photoreduction of Cr^{VI} ions in a Pyrex inner-irradiation-type reaction vessel connected to a glass closed gas-circulation system.[11] The metal oxide or metal-loaded sample (0.25 g) was then dispersed in aqueous K_2CrO_4 solution (370–400 mL, 0.18–0.23 mM). The pH of the solution was not adjusted ($pH\approx7.5$) unless otherwise stated. After evacuation, the solution was exposed to visible irradiation ($\lambda>400$ nm) to reduce Cr^{VI} to Cr^{III}. Irradiation was conducted using a 450 W high-pressure Hg lamp (UM-452, Ushio) and a Pyrex tube filled with aqueous sodium nitrite solution as a filter to block ultraviolet light.[16] During visible-light irradiation, H_2 and O_2 evolution were observed simultaneously, which indicates that water splitting did occur.[11b] Visible-light irradiation was typically performed for 4–8 h, until the rates of H_2 and O_2 evolution become stoichiometric; that is, overall water splitting was achieved (or, in other words, the photoreduction of Cr^{VI} ceased).[11b] The temperature of the reactant solution was maintained at room temperature by a flow of cooling water during the preparation procedure. The final product was washed well with distilled water and dried overnight at 343 K.

Characterisation of materials: The prepared samples were studied by HR-TEM (JEM-2010F, Jeol), SEM (S-4700, Hitachi) and XAFS. XAFS measurements were carried out at the BL01B1 beamline of the SPring-8 synchrotron facility (Hyogo, Japan) using a ring energy of 8 GeV and a stored current of 100 mA in top-up mode (proposal nos. 2004B0075-NXa-np and 2007A1803) and at the BL12C and NW-10A beamlines of the Photon Factory (High-Energy Accelerator Research Organization, Tsukuba, Japan) using a ring energy of 2.5 GeV and a stored current of 450–300 mA (proposal nos. 2004G317, 2006G125, 2007G624, and 2008G150). The spectra were measured in transmission or fluorescence mode at room temperature using a Si(111) two-crystal monochromator. Data reduction was performed using the REX2000 program (Rigaku Corporation). The photon energies in the XANES spectra were corrected with reference to Cu foil (8980.3 eV).

Visible-light water-splitting reaction: Photocatalytic reactions were carried out using the same experimental setup as that used for the preparation of the Rh/Cr_2O_3 (core–shell) nanoparticles. The reactant solution, consisting of catalyst (0.15 g) and pure water (370–400 mL), was evacuated several times prior to reaction to ensure that no air remained in the reaction vessel. The reactant solution was maintained at room temperature by a flow of cooling water during the reaction. The evolved gases were analyzed by a gas chromatograph connected directly to the closed gas-circulation system. The reproducibility of the rates of H_2 and O_2 evo-

lution in this system was confirmed to be within approximately 10% under the same reaction conditions.

Acknowledgements

The authors thank the staff of Mitsubishi Chemicals Co. for the elemental analysis. This work was supported by the 21st Century Center of Excellence (COE) and the Research and Development in a New Interdisciplinary Field Based on Nanotechnology and Materials Science programs of the Ministry of Education, Culture, Sports, Science and Technology (MEXT) of Japan. One of the authors (K.M.) gratefully acknowledges the support of a Japan Society for the Promotion of Science (JSPS) Fellowship. Acknowledgement is also extended to the KAITEKI Institute, Inc, the Global Center of Excellence (GCOE) Program for Chemistry Innovation through Cooperation of Science and Engineering and Nippon Sheet Glass Foundation for Materials Science and Engineering.

[1] A. J. Bard, M. A. Fox, *Acc. Chem. Res.* **1995**, *28*, 141.
[2] J. S. Lee, *Catal. Surv. Asia* **2005**, *9*, 217.
[3] R. Abe, K. Sayama, H. Sugihara, *J. Phys. Chem. B* **2005**, *109*, 16052.
[4] a) P. G. Hoertz, T. E. Mallouk, *Inorg. Chem.* **2005**, *44*, 6828; b) W. J. Youngblood, S.-H. A. Lee, K. Maeda, T. E. Mallouk, *Acc. Chem. Res.* **2009**, *42*, 1966.
[5] K. Maeda, K. Domen, *J. Phys. Chem. C* **2007**, *111*, 7851.
[6] F. E. Osterloh, *Chem. Mater.* **2008**, *20*, 35.
[7] Y. Inoue, *Energy Environ. Sci.* **2009**, *2*, 364.
[8] A. Kudo, Y. Miseki, *Chem. Soc. Rev.* **2009**, *38*, 253.
[9] D. Gust, T. A. Moore, A. L. Moore, *Acc. Chem. Res.* **2009**, *42*, 1890.
[10] a) H. Hata, Y. Kobayashi, V. Bojan, W. J. Youngblood, T. E. Mallouk, *Nano Lett.* **2008**, *8*, 794; b) R. Ma, Y. Kobayashi, W. J. Youngblood, T. E. Mallouk, *J. Mater. Chem.* **2008**, *18*, 5982.
[11] a) K. Maeda, K. Teramura, D. Lu, N. Saito, Y. Inoue, K. Domen, *Angew. Chem.* **2006**, *118*, 7970; *Angew. Chem. Int. Ed.* **2006**, *45*, 7806; b) K. Maeda, K. Teramura, D. Lu, N. Saito, Y. Inoue, K. Domen, *J. Phys. Chem. C* **2007**, *111*, 7554.
[12] a) K. Maeda, D. Lu, K. Teramura, K. Domen, *J. Mater. Chem.* **2008**, *18*, 3539; b) K. Maeda, D. Lu, K. Teramura, K. Domen, *Energy Environ. Sci.* **2010**, *3*, 471.
[13] N. Sakamoto, H. Ohtsuka, T. Ikeda, K. Maeda, D. Lu, M. Kanehara, K. Teramura, T. Teranishi, K. Domen, *Nanoscale* **2009**, *1*, 106.
[14] a) K. Maeda, K. Teramura, D. Lu, T. Takata, N. Saito, Y. Inoue, K. Domen, *Nature* **2006**, *440*, 295; b) K. Maeda, K. Teramura, H. Masuda, T. Takata, N. Saito, Y. Inoue, K. Domen, *J. Phys. Chem. B* **2006**, *110*, 13107; c) K. Maeda, K. Teramura, D. Lu, T. Takata, N. Saito, Y. Inoue, K. Domen, *J. Phys. Chem. B* **2006**, *110*, 13753; d) K. Maeda, K. Teramura, N. Saito, Y. Inoue, K. Domen, *J. Catal.* **2006**, *243*, 303; e) K. Maeda, H. Masuda, K. Domen, *Catal. Today* **2009**, *147*, 173.
[15] M. Yoshida, K. Takanabe, K. Maeda, A. Ishikawa, J. Kubota, Y. Sakata, Y. Ikezawa, K. Domen, *J. Phys. Chem. C* **2009**, *113*, 10151.
[16] a) K. Maeda, T. Takata, M. Hara, N. Saito, Y. Inoue, H. Kobayashi, K. Domen, *J. Am. Chem. Soc.* **2005**, *127*, 8286; b) K. Maeda, K. Teramura, T. Takata, M. Hara, N. Saito, K. Toda, Y. Inoue, H. Kobayashi, K. Domen, *J. Phys. Chem. B* **2005**, *109*, 20504.
[17] H. Kato, A. Kudo, *J. Phys. Chem. B* **2001**, *105*, 4285.
[18] a) S. Bordiga, F. Bosherini, S. Coluccia, F. Genoni, C. Lamberti, G. Leofanti, L. Marcheses, G. Petrini, G. Vlaic, A. Zecchina, *Catal. Lett.* **1994**, *26*, 195; b) B. M. Weckhuysen, R. A. Schoonheydt, J. M. Jehng, I. E. Wachs, S. J. Cho, R. Ryoo, S. Kijlstra, E. Poels, *J. Chem. Soc. Faraday Trans.* **1995**, *91*, 3245.
[19] K. Domen, S. Naito, M. Soma, T. Onishi, K. Tamaru, *J. Chem. Soc. Chem. Commun.* **1980**, 543.
[20] J. M. Lehn, J. P. Sauvage, R. Ziessel, *Nouv. J. Chim.* **1980**, *4*, 623.
[21] K. Teramura, K. Maeda, T. Saito, T. Takata, N. Saito, Y. Inoue, K. Domen, *J. Phys. Chem. B* **2005**, *109*, 21915.
[22] D. R. Lide, *Handbook of Chemistry and Physics*, 83rd ed., CRC Press, Boca Raton, **2002**.
[23] J. F. Reber, K. Meier, *J. Phys. Chem.* **1986**, *90*, 824.
[24] B. Ohtani, K. Iwai, S. Nishimoto, S. Sato, *J. Phys. Chem. B* **1997**, *101*, 3349.
[25] N. Bao, L. Shen, T. Takata, K. Domen, *Chem. Mater.* **2008**, *20*, 110.
[26] K. Maeda, M. Eguchi, S.-H. A. Lee, W. J. Youngblood, H. Hata, T. E. Mallouk, *J. Phys. Chem. C* **2009**, *113*, 7962.
[27] M. Yoshida, A. Yamakata, K. Takanabe, J. Kubota, M. Osawa, K. Domen, *J. Am. Chem. Soc.* **2009**, *131*, 13218.
[28] J.-P. Zhang, D.-Z. Sun, X.-B. Li, X.-L. Wang, M.-Y. Kong, Y.-P. Zeng, J.-M. Li, L.-Y. Lin, *J. Cryst. Growth* **1999**, *201/202*, 429.
[29] M.-I. Baraton, K. E. Gonsalves, *J. Cluster Sci.* **1999**, *10*, 133.
[30] It was confirmed by XANES analysis that the absorption profile of the prepared sample was very similar to that of the Rh_2O_3 reference and was clearly different from that of the sample prepared by reduction with H_2 (see Figure S7 in the Supporting Information).
[31] A. Kudo, S. Nakagawa, H. Kato, *Chem. Lett.* **1999**, 1197.

Received: March 10, 2010
Published online: June 16, 2010

